

Full length article

Imperfection sensitivity analysis and DSM design of web-stiffened lipped channel columns experiencing local-distortional interaction

Lu Deng, Jiaoli Li, Yuanliang Yang, Peng Deng*

Key Laboratory for Damage Diagnosis of Engineering Structures of Hunan Province, Hunan University, Changsha, 410082, China



ARTICLE INFO

Keywords:

Cold-formed steel column
Local-distortional (L-D) interactive failure
Load-carrying capacity
Initial imperfection
Direct strength method (DSM)

ABSTRACT

Cold-formed thin-walled steel members are commonly subjected to initial imperfection, which will greatly affect their load-carrying capacity. In this study, the load-carrying capacity and imperfection sensitivity of fixed-ended cold-formed steel web-stiffened lipped channel columns subjected to local-distortional (L-D) interactive failure (including secondary local bifurcation interaction (SLI), true L-D interaction (TI) and secondary distortional bifurcation interaction (SDI)) are investigated. A new imperfection simulation method combining finite element analysis (FEA) with the constrained finite strip method (cFSM) was firstly proposed, and then validated using experimental data from literatures. Next, 224 geometries of columns experiencing L-D interactive failure were chosen by the cFSM and their load-carrying capacity under normal state P_{num} (with unavoidable minor initial imperfection) and those under imperfect state $P_{imperfect}$ (with various imperfections) were respectively obtained using FEA. The most unfavorable imperfection patterns for L-D interactive failure were summarized by comparing the $P_{imperfect}$ and P_{num} of the members. Furthermore, the quality of the DSM-based design approaches for L-D interactive failure were evaluated by comparing P_{num} with the failure load predictions of the selected columns provided by these design approaches.

1. Introduction

In recent years, cold-formed thin-walled steel has been widely applied in residential buildings, industrial factory buildings, storage racks and other fields due to its characteristics of lightweight and high strength [1,2]. Web-stiffened lipped channel (WSLC, as shown in Fig. 1), as one of the most widely used section forms at present, greatly improves the load-carrying capacity of members due to its 'v-shaped' stiffeners on the web. The presence of stiffeners will dramatically change the failure mode of the members, especially for the members experiencing coupled buckling failure [3]. This work presents the load-carrying capacity of WSLC columns subjected to L-D interactive failure (including secondary local bifurcation interaction (SLI), true L-D interaction (TI) and secondary distortional bifurcation interaction (SDI)) [4].

When it comes to the WSLC members experiencing L-D interactive failure, finite element analysis (FEA) and direct strength method (DSM) are commonly used. As an important influencing factor, the initial imperfection simulation cannot be ignored in the FEA. It is well known that initial imperfections can be easily induced in cold-formed thin-walled steel members in the process of cold-rolling production, transportation and installation. The initial imperfections mainly include

initial geometric imperfection and residual stress, while the latter can usually be ignored as it is reckoned that it has little impact on the load-carrying capacity of the components [5,6]. The existence of initial imperfection will greatly reduce the load-carrying capacity of cold-formed steel members and may even change the failure modes of the members [7]. It has been shown that the reduction of the load-carrying capacity caused by initial geometric imperfection can reach up to 35.91% when compared with the perfect members [8]. Therefore, it is necessary as well as important to consider the initial imperfection when studying the cold-formed steel members experiencing the L-D interactive failure.

Many different imperfection simulation methods have been proposed. Generally, the initial imperfection field (consists of all imperfections on the entire member) can be presented as a combination of basic imperfection shapes at different magnitudes. For instance, the first buckling mode method uses the first buckling mode as the imperfection shape and the corresponding recommended value [9–11] as the imperfection amplitude to generate the initial imperfection field of the cold-formed steel members. The mode combination method proposed by Dinis & Camotim [12] adopted several basic buckling modes with different participation ratios as the initial geometric imperfection of the

* Corresponding author.

E-mail addresses: denglu@hnu.edu.cn (L. Deng), JiaoliLi.hnu@outlook.com (J. Li), yangyl@hnu.edu.cn (Y. Yang), dengpeng@hnu.edu.cn (P. Deng).

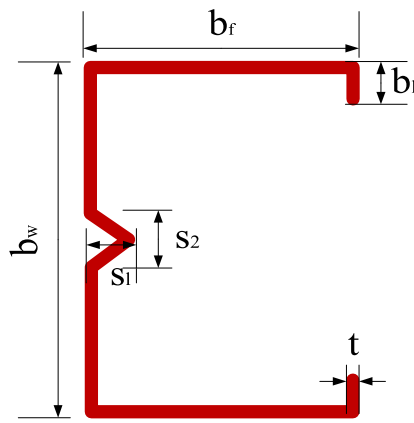


Fig. 1. Web-stiffened lipped channel section.

members. Moreover, the imperfection simulation method proposed by Bonada [13] firstly selected a few low-order FEM buckling modes with different participation ratios in simulating the imperfection shape, and then determined the imperfection amplitude-based the buckling mode decomposition results obtained from the generalized beam theory (GBT). It should be noted that the accuracy and limitations of different simulation methods are also different when calculating the load-carrying capacity of cold-formed steel members. One of the main reasons could be that the selection of basic imperfection shapes among most of these imperfection simulation methods is simply based on the visual judgment of the buckling modes obtained from finite element analysis (FEA). As such, they usually fail to fully consider all the imperfection shapes that have important influence on the load-carrying capacity of members, leading to an overestimation of the load-carrying capacity [13]. In contrast, the mode combination method tends to have conservative results since it adopts a large number of imperfection fields at the cost of huge computational demand. Moreover, simulation methods that are directly applicable to WSLC sections affected by L-D interactive are rare. Therefore, it is of significant importance to develop reasonable imperfection simulation models for WSLC members experiencing L-D interactive failure, which will be helpful to investigate the imperfection sensitivity of cold-formed members and verify the accuracy of the existing direct strength method (DSM).

As the most popular design method to predict the load-carrying capacity of cold-formed steel members, the DSM was initially proposed by Schafer [14] for studying cold-formed thin-walled members with plain cross-section assumption. With the further study of coupled buckling failure, some modified formulas for L-D failure were developed. Based on DSM, Schafer [15] subsequently proposed the NLD method and the NDLC method to predict the L-D interactive failure. Besides, for the TI and SDI failures, the generalized modified NDLC approach (MNDLC) and a novel DSM-based approach termed NSDB method were proposed by Silvestre et al. [16] and Martins et al. [4], respectively. The applicability of these design approaches to study the WSLC columns with the failure mode of L-D interactive buckling has been verified by both experimental or numerical results [3,17–19], but a comprehensive comparison of all the design approaches is still absent so far, which may cause inconvenience and confusion in the application of these methods for practical design.

In this paper, a new imperfection simulation method for WSLC members experiencing L-D interactive failure was firstly proposed. The accuracy of the proposed imperfection simulation method was verified by comparing with experimental results [20–23]. Then, FEA was used to analyze 224 members subjected to L-D interactive failure with the help of the proposed imperfection simulation method. In addition, comparing the load-carrying capacity of 224 members with various imperfections and their FEA results, the most unfavorable imperfection shapes of members subjected to the three types of L-D interactive failure as well as the reduction of each imperfection shape to the load-carrying capacity

were obtained. Finally, the applicability and accuracy of the design approaches were evaluated by comparing those predictions provided by the design approaches with FEA results. The main research process can be seen in Fig. 2. This work will help guide the design and application of cold-formed steel members.

2. Imperfection simulation method

The buckling modes of the members, obtained by ABAQUS [24] buckling analysis, were utilized as the basic participation shapes of the imperfection field. Through the constrained finite strip method (cFSM) analysis, ‘pure’ buckling modes were derived and then buckling mode decomposition of the WSLC members was conducted [25]. Finally, the initial imperfection field of the WSLC columns was obtained by combining FEA and cFSM. The detailed descriptions of imperfection simulation are as follows.

2.1. Mode buckling analysis by FEA

The buckling modes of the WSLC columns were analyzed by using the ABAQUS software. These buckling modes were used as the components of the imperfection field. The buckling eigenvalues were used to determine the proportion of the corresponding buckling modes in the imperfection field and the imperfection amplitude. In this study, the first ten buckling modes and corresponding eigenvalues of the WSLC columns were selected. Basic information regarding the FE model is introduced as follows:

Element and mesh: S4R shell element was adopted due to the fact that the thickness of cold-formed steel sections is usually less than 2mm. The minimum size of the elements was set at 5–10mm, while an aspect ratio between 1/2 and 2 was kept to ensure the accuracy of finite element analysis [26].

Material properties: The material property for the whole cross-section was assumed homogeneous and isotropic. An elastic/perfectly-plastic stress-strain law was adopted as the constitutive relation with different Young’s modulus E and yield strength F_y while keeping Poisson’s ratio $\nu = 0.3$.

Boundary conditions and the load: All the nodes of the end sections were coupled at the centroid of the section (as shown in Fig. 3). At the centroid points of two end sections, except for the degrees of freedom in the loading direction, the other eleven degrees of freedom of the WSLC columns were constrained. At the same time, an axial force of 1 N was applied at the centroid of the loading end to complete the application of external load. Finally, the boundary conditions of the WSLC columns and application of external load were related to the centroid of the end section.

2.1.1. cFSM section analysis

At present, cFSM is one of the main methods to conduct cross-section analysis. The CUFSM program was used to get the five ‘pure’ buckling modes of the cross-section. The buckling shapes in the longitudinal distribution are sinusoidal, and the critical buckling half-wavelengths were used as longitudinal half-wavelengths. The five ‘pure’ buckling modes which include ‘pure’ distortional, local, major axis flexural, minor axis flexural and torsional buckling modes of the whole member (recorded as D, L, G_{major} , G_{minor} , G_{torque}) and their half-wavelengths (recorded as $\frac{1}{2}\lambda_D$, $\frac{1}{2}\lambda_L$, $\frac{1}{2}\lambda_{G_{major}}$, $\frac{1}{2}\lambda_{G_{minor}}$, $\frac{1}{2}\lambda_{G_{torque}}$) are shown in Fig. 4.

2.1.2. Mode decomposition and identification

The ‘pure’ buckling modes obtained by the CUFSM program was used to decompose the buckling modes of the members. Finally, the buckling mode of the members was decomposed into several ‘pure’ buckling modes using Matlab, i.e.:

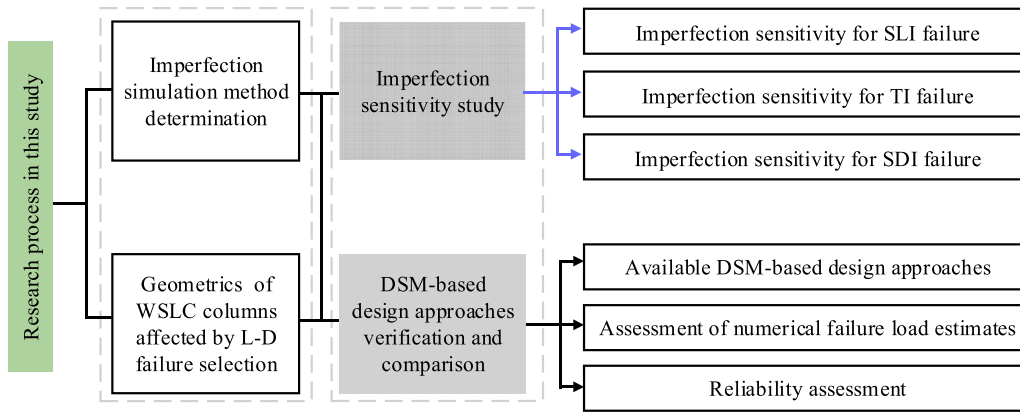


Fig. 2. Research process in this study.

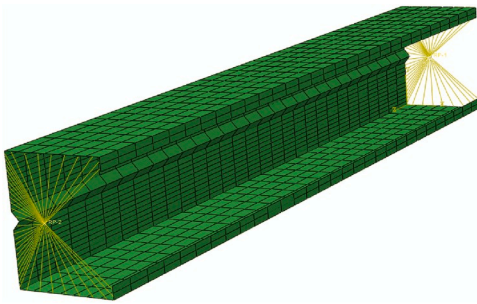


Fig. 3. Boundary conditions and meshing scheme.

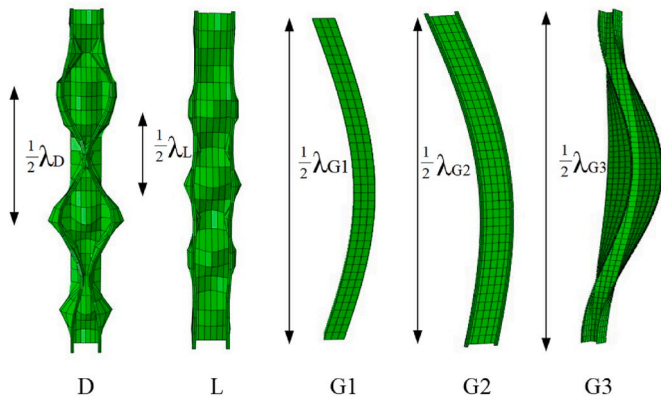


Fig. 4. Five ‘pure’ buckling mode shapes and their buckling half-wavelengths.

$$f(x, y, z) = \sum_{i=1}^5 \alpha_i \phi_i(x, y, z) \quad (1)$$

where f represents buckling modes obtained from FEM; the coefficient α_i represents the degree of mode participation; ϕ_i represents the basic ‘pure’ buckling mode.

In order to facilitate the buckling mode decomposition, the distributions of section intermediate nodes in the CUFSM were adopted to be similar with the ABAQUS shell FEA, which led to a huge increase in the number of basic buckling modes, especially for local buckling modes. The number of global, distortional and local buckling modes calculated by the cFSM are 4, $nm-4$, $nm+2ns+2$ (nm : the number of main cross-section nodes, ns : the number of sub-nodes located between main nodes, the locations of nm and ns are show in Fig. 5(a)), respectively, and the basic buckling modes of shear deformation are ignored [27]. Therefore, it is necessary to select modes that have a practical influence

on the load-carrying capacity within the five basic buckling modes. Moreover, the longitudinal half-wavelength number of local and distortional buckling mode obtained from CUFSM should be consistent with the ABAQUS buckling modes, which is very important for the accuracy and effectiveness of the subsequent mode identification.

According to Eq. (1), the buckling modes of the members were decomposed to obtain their composition. The displacement degrees of freedom (DOFs) of CUFSM mode base should be consistent with that of ABAQUS model, as the fields of DOFs obtained from CUFSM and ABAQUS are different in dimension and reality meanings. The field of displacement DOFs obtained by FEA consists of three displacement DOFs of each node in the WSLC columns, which represents the displacements of each node in the x , y and z directions of the Cartesian coordinate system, respectively. While the displacement DOFs field obtained from finite strip analysis (as show in Fig. 5(b)) is comprised of four displacement DOFs of each node, the displacement field includes the displacement U and V in the thin plate, the displacement W that perpendicular to the thin plate and the rotation θ of node [28]. Therefore, the mode decomposition can only be implemented after the substitution of the two fields of displacement DOFs, which is of great significance for the feasibility and correctness of mode decomposition.

2.2. Imperfection field generation by combing FEA and cFSM

Taking the column ($b_1 = 16.6$ mm, $b_f = 62$ mm, $b_w = 105.3$ mm, $S_1 = 19.6$ mm, $S_2 = 9.9$ mm, $t = 1.205$ mm, $L = 2402$ mm) as an example, the first 10 buckling modes and their corresponding eigenvalues were obtained by FEA. Using the cFSM to conduct mode decomposition and identification, and the proportion of ‘pure’ global, local and distortional buckling mode (distortional buckling mode includes symmetric and anti-symmetric shape) in each buckling mode were obtained. The magnitudes of the 10 buckling modes are determined using the values adopted by Bonada [13] (take $b_w/200$, $b_f/50$ and, $L/1000$ as the

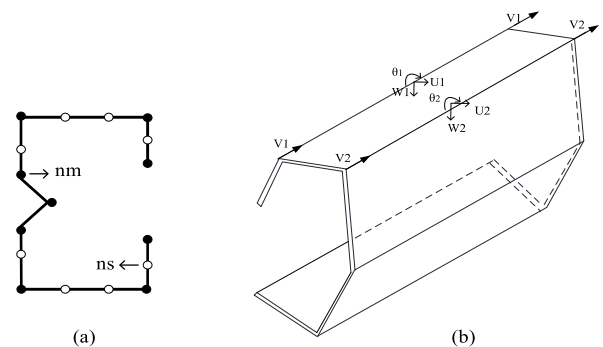


Fig. 5. Discretized cross-section and displacements notation used in cFSM analysis.

Table 1
The first 10 buckling modes, corresponding eigenvalues and the results of cFSM mode identification.

Buckling modes	Eigenvalues (N)	The proportion of				Buckling mode Magnitudes (mm)
		'Pure' G	'Pure' L	'Pure' SD	'Pure' AD	
1	8.3 E+04	0.50%	21.84%	77.66%	0.00%	1.090
2	8.5 E+04	0.09%	30.37%	69.54%	0.00%	1.024
3	1.10E+05	0.32%	3.76%	95.85%	0.07%	1.216
4	1.14E+05	2.22%	4.83%	88.53%	4.42%	1.177
5	1.15E+05	98.24%	0.00%	1.75%	0.00%	2.381
6	1.17E+05	0.26%	89.88%	1.64%	8.21%	0.500
7	1.17E+05	0.24%	81.01%	1.90%	16.84%	0.456
8	1.17E+05	0.08%	88.42%	3.41%	8.08%	0.510
9	1.17E+05	0.04%	95.62%	3.55%	0.80%	0.548
10	1.17E+05	0.23%	80.51%	1.72%	17.54%	0.451

'Pure' SD/AD: pure symmetric/anti-symmetric distortional buckling modes.

Table 2
The imperfection filed, including: (a) buckling modes and (b) their corresponding proportions in the imperfection field, (c) the amplitude of the imperfection field.

Selected buckling mode(a)	Eigenvalue (N)	Reciprocal of the eigenvalue	The proportions of		Buckling mode magnitude (mm)
			Mode ^(b)	Mode magnitude	
1	8.30E+04	1/8.30E+04	100.00%	31.34%	1.090
3	1.10E+05	1/1.10E+05	75.83%	23.77%	1.216
5	1.15E+05	1/1.15E+05	72.15%	22.61%	2.381
6	1.17E+05	1/1.17E+05	71.09%	22.28%	0.500
The imperfection amplitude of the imperfection field ^(c)					1.280

amplitude of 'pure' L, D and G buckling mode) in proportion to results of mode identification. The buckling modes and their corresponding eigenvalues, as well as the results of cFSM mode decomposition and identification are shown in Table 1.

The ABAQUS buckling modes whose maximum participation differences are greater than 10% were selected to constitute the imperfection field of the WSLC members (as show in Table 2). The shapes and amplitudes of the imperfection fields were determined by superimposing the selected buckling modes and their amplitudes proportionally, respectively. Furthermore, the ratios of the buckling modes and corresponding amplitudes in the imperfection filed were obtained through dividing the reciprocals of the selected mode eigenvalues by their counterparts in Mode 1 and their sum, respectively. The process of imperfection fields' generation has been presented in Fig. 6.

3. Validation of imperfection simulation method

The nonlinear analysis was conducted on the 40 experimental fixed-ended WSLC columns (shown in Table 3) affected by L–D interaction in existing literatures [20–23] to obtain their load-carrying capacity. The material properties of those columns are shown in Table 4. The accuracy of the imperfection simulation method proposed in this paper can be validated by comparing the FEA results with the experimental loads. The FEA model setup programs such as element, mesh, property and boundary conditions are consistent with the buckling analysis. Static Riks was used to perform non-linear analysis. Moreover, the majority convergence requirements of load-carrying capacity calculation could be met if the number of iteration steps reaches 120. The imperfection fields of the members were introduced into the FEA models before conducting the nonlinear analysis.

It should be noted that there are various suggested values on the imperfection amplitudes in existing studies besides the group of amplitudes adopted in section 2. For example, 0.1t and L/1000 have been commonly taken as the section imperfection and the global imperfection amplitude of the columns, respectively [3,11,12]. Schafer [10] summarized the cumulative distribution function (CDF) values based on the collected data on geometric imperfections and recommended values for the imperfection amplitudes. Moreover, the design standards for cold-formed steel such as European Standard EN 1993-1-5: 2006/AC: 2009 [29] and North American Specification AISI-S100 [30] also provide suggestions regarding the imperfection amplitudes. As such, no consensus has yet been reached on the recommended imperfection amplitudes.

Different imperfection amplitudes will result in different nonlinear analysis accuracy, as cold-formed thin-walled members are sensitive to the imperfection [31]. The load-carrying capacity of columns was calculated under different recommend imperfection amplitudes. In addition to the group of amplitudes that Bonada adopted ($b_w/200$, $b_f/50$ and $L/1000$ were taken as the amplitude of L, D, and G buckling mode), Table 5 also presented the other four groups of imperfection amplitudes and their calculation results. As the results shown in Table 5, when taking 0.1t, 0.1t and L/1000 as the amplitude of L, D, and G buckling mode, both average and standard deviation performed better than the other groups. Therefore, the fourth set of recommended amplitudes was taken in this study.

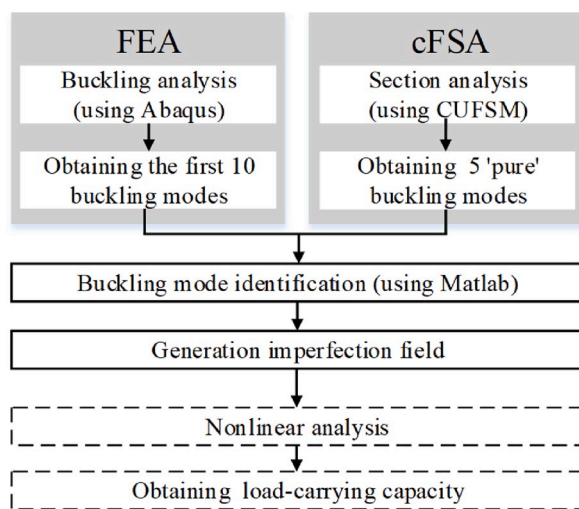


Fig. 6. Imperfection field generation process.

Table 3
Geometry dimensions and their failure loads of the WSLC type columns experiencing L-D interaction in available literature.

No.	b_l (mm)	b_f (mm)	b_w (mm)	L (length) (mm)	S_1 (mm)	S_2 (mm)	T (mm)	P_{Exp} (kN)
1	10	40	40	400	12	6	0.60	17.98
2	10	40	40	1000	12	6	0.60	12.38
3	10	40	40	1200	12	6	0.60	25.87
4	10	40	80	800	14	7	0.60	23.50
5	10	40	80	1000	14	7	0.60	18.74
6	10	40	80	1200	14	7	0.60	21.87
7	10	50	50	800	12	6	0.80	40.32
8	10	50	50	1000	12	6	0.80	32.59
9	12	65	120	700	20	10	1.07	71.41
10	12	65	120	1000	20	10	1.07	58.75
11	12	65	120	1300	20	10	1.07	56.47
12	12	65	120	2000	20	10	1.07	47.69
13	15	125	163	1001	22	10	1.48	114.20
14	16	125	163	1000	22	11	1.49	116.50
15	16	124	164	1001	22	9	1.47	110.90
16	16	125	165	1501	21	12	1.48	97.50
17	17	123	163	1502	20	10	1.47	92.80
18	14	123	165	1501	20	10	1.48	95.10
19	16	125	166	1999	22	10	1.46	84.80
20	16	125	164	2003	21	11	1.49	97.00
21	15	125	164	2001	22	11	1.47	89.30
22	21	123	163	1002	21	10	1.48	125.80
23	23	124	162	999	20	10	1.49	133.10
24	23	123	163	999	21	11	1.49	131.30
25	21	126	162	1500	19	10	1.47	98.60
26	21	124	163	1502	20	10	1.47	100.30
27	21	125	163	1501	22	11	1.47	101.20
28	21	124	164	2001	22	10	1.46	92.50
29	21	123	165	2002	23	10	1.45	86.80
30	21	123	164	2002	22	11	1.47	98.50
31	17	52	97	2097	20	11	1.01	63.26
32	17	57	106	2499	20	11	1.01	59.80
33	17	57	107	2500	20	10	0.99	58.99
34	17	62	105	2702	19	10	1.00	57.51
35	17	62	115	3001	20	10	1.00	55.93
36	17	57	101	2147	20	10	1.20	83.16
37	17	62	105	2402	20	10	1.21	83.37
38	17	62	106	2402	20	10	1.20	80.86
39	17	67	112	2701	20	10	1.19	75.51
40	17	67	118	2820	19	10	1.23	77.88

Note: No.1–8 are from Ref. [20], No.9–12 are from Ref. [21], No.13–30 are from Ref. [22] and No. 31–40 are from Ref. [23].

Table 4
Measured material properties of the 40 columns in available literature.

No.	Yield stress F_y (MPa)	Ultimate stress F_u (MPa)	Young's modulus E (MPa)	Poisson's ratio ν	Elongation (%)
1–6	627.7	632.8	2.00E+5	0.3	12.8
7–8	632.8	646.4	2.00E+5	0.3	9.4
9–12	634.0	\	2.17E+5	0.3	\
13–30	435	500	1.99E+5	0.3	25.81
31–35	550	606	2.16E+5	0.3	\
36–40	500	591	2.14E+5	0.3	\

In addition, the other available imperfection simulation methods were also used to obtain the FEA results of 40 experimental data respectively. The calculation accuracy of each method is shown in Table 6. Obviously, compared with the first buckling mode method and Bonada's method, the

Table 5
The recommended values of imperfection amplitudes and their calculation errors relative to experimental members.

No.	Imperfection magnitude			Average of P_{FEM}/P_{Exp}	Standard deviation of P_{FEM}/P_{Exp}	Error (%)
	'Pure' L	'Pure' D	'Pure' G			
1 [13]	$b_w/200$	$b_f/50$	$L/1000$	1.083	0.070	8.3
2 [10]	$0.34t$	$0.94t$	$L/1000$	1.089	0.069	8.9
3 [10]	$0.50t$	$1.29t$	$L/1000$	1.119	0.071	11.9
4 [3]	$0.10t$	$0.10t$	$L/1000$	1.037	0.047	3.7
5 [10]	$0.006b_w$	$1.00t$	$L/750$	1.100	0.068	10.0

P_{FEM} , P_{Exp} : the load-carrying capacity obtained by FEA and experiment, respectively.

method in this article and Camotim's are more accurate. For the two methods that perform better in accuracy, the calculation workload of the proposed method is dramatically smaller than that in Camotim's method, although the buckling modes that combined with the imperfection filed in the proposed method are usually larger than that in Camotim's method, and the latter only use critical local and distortional mode to generate the

Table 6
The accuracy of different imperfection simulations for load-carrying capacity.

P_{FEM}/P_{Exp}	First buckling mode method	Camotim's method	Bonada's method	The method in this article
Average	1.109	0.968	1.106	1.037
Standard deviation	0.071	0.042	0.068	0.047
Error (%)	10.9	3.2	10.6	3.7

imperfection filed. Since only one imperfection field needs to be considered for each component using the method proposed in this work, which is dramatically smaller than that in the Camotim’s method. Therefore, it can be seen that the method proposed in this work is not only of high accuracy but also timesaving.

4. Column selection

In order to investigate the imperfection sensitivity and evaluate design approaches of fixed-ended WSLC columns affected by L-D interaction, the CUFISM program was used to determine the column geometries of 28 sections affected by L-D interaction. The failure modes of thin-walled members were determined by the ratio of the critical distortional buckling load to the critical local buckling load P_{crD}/P_{crL} , critical global buckling load to critical local or distortional load $P_{crG}/P_{cr,max}$ ($P_{cr,max} = \max(P_{crD}, P_{crL})$) and critical global buckling load to yield load P_{crG}/P_y . It requires (1) $0.4 < P_{crD}/P_{crL} < 0.8$, $0.8 < P_{crD}/P_{crL} < 1.3$, $1.3 < P_{crD}/P_{crL} < 2.4$ for SLI, TI and SDI, respectively and ensures (2) $P_{crG}/P_{cr,max} > 5.2$, (3) $P_{crG}/P_y > 1.1$ [4]. After the calculation of critical buckling strengths and adjustment of column geometries using CUFISM, the geometries of 28 WSLC columns (as shown in Table 7) were determined. Moreover, the yield strength F_y was adopted within 400–750 to avoid narrow critical slenderness λ_{cr} ($\lambda_{cr} = (P_y/P_{cr})^{0.5}$) values range. Finally, 224 WSLC columns (for the 28 WSLC columns geometry, 8 yield strengths per column geometry) experiencing L-D interaction were obtained. The material properties were set as Young’s modulus $E = 210,000$ MPa and Poisson’s ratio $\nu = 0.3$.

The load-carrying capacity of the 224 WSLC columns were obtained by FEA (P_{num}) with the help of the imperfection simulation method proposed in this paper. The results of FEA could be seen as the load-carrying capacity of the members under normal state, which will be used to measure the impact of imperfection on members as well as the accuracy of the DSM-based design approaches. It should be noted that the research and corresponding conclusions in this work only refer to the cold-formed thin-walled steel column with a specific intermediate web stiffeners size, since for all columns involved in the analysis, the dimensions of the intermediate web stiffeners are almost invariable settings ($S_1 = 10$ mm, $S_2 = 20$ mm), except for a few columns ($S_1 = 15$ mm, $S_2 = 30$ mm). For the cold-formed thin-walled steel columns with other intermediate web stiffeners size

Table 7
The selected geometries and critical loads of WSLC columns affected by L-D interaction.

No.	b_l (mm)	b_t (mm)	b_w (mm)	L (length) (mm)	S_1 (mm)	S_2 (mm)	T (mm)	P_{crL} (kN)	P_{crD} (kN)	P_{crG} (kN)	P_{crD}/P_{crL}
WSLC1	8	100	120	1800	10	20	1.4	89.30	42.74	488.74	0.5
WSLC2	8	100	120	1500	10	20	1.4	89.30	45.54	558.83	0.5
WSLC3	8	100	120	1400	10	20	1.4	89.32	45.74	641.19	0.5
WSLC4	8	100	120	1000	10	20	1.4	89.57	55.12	1254.64	0.6
WSLC5	8	100	120	800	10	20	1.4	89.93	59.08	1959.15	0.7
WSLC6	8	90	100	1400	10	20	1.0	35.98	25.13	292.23	0.7
WSLC7	8	90	100	1200	10	20	1.0	35.99	27.15	397.44	0.8
WSLC8	12	85	130	1500	10	20	1.2	75.39	57.76	531.68	0.8
WSLC9	12	85	130	1400	10	20	1.2	75.38	60.73	610.11	0.8
WSLC10	8	90	100	900	10	20	1.0	36.09	32.07	705.89	0.9
WSLC11	12	85	130	1000	10	20	1.2	75.48	71.62	1194.28	0.9
WSLC12	10	80	80	1500	10	20	0.8	20.99	22.36	176.09	1.1
WSLC13	12	85	130	900	10	20	1.2	75.58	75.63	1474.04	1.0
WSLC14	12	85	130	800	10	20	1.2	75.69	83.48	1865.15	1.1
WSLC15	10	120	160	1300	15	30	1.1	37.66	45.40	1278.26	1.2
WSLC16	15	100	120	1300	10	20	1.2	59.85	75.42	726.46	1.3
WSLC17	15	100	120	1200	10	20	1.2	59.88	77.78	852.36	1.3
WSLC18	10	80	80	900	10	20	0.8	21.02	29.44	349.44	1.4
WSLC19	15	100	120	1000	10	20	1.2	59.98	89.52	1226.85	1.5
WSLC20	15	120	150	1400	10	20	1.0	28.54	45.86	917.85	1.6
WSLC21	20	100	150	1500	10	20	1.1	50.45	85.92	841.92	1.7
WSLC22	20	100	150	1400	10	20	1.1	50.46	90.67	966.35	1.8
WSLC23	15	80	100	1200	10	20	0.8	23.12	43.49	347.21	1.9
WSLC24	20	150	180	1500	15	30	1.3	50.30	100.57	1925.33	2.0
WSLC25	20	100	150	1200	10	20	1.1	50.50	107.20	1314.96	2.1
WSLC26	15	80	100	1000	10	20	0.8	23.13	50.99	499.77	2.2
WSLC27	20	120	180	1200	10	20	1.2	53.51	122.16	2305.26	2.3
WSLC28	15	120	150	1000	10	20	1.0	28.68	68.61	1798.38	2.4

settings, it should be further investigated.

5. Imperfection sensitivity analysis

Previous studies shows that only when the imperfection shapes are close to the buckling shapes of the members can the load-carrying capacity of the members be greatly weakened and even the failure state of the members be changed [32,33]. In order to investigate the influence of various initial imperfections on the load-carrying capacity of the fixed-ended columns affected by L-D interaction failure, the basic ‘pure’ buckling modes with four different amplitudes in Table 8 (based on the cumulative distribution function values in Ref. [10]) are introduced into the WSLC columns as initial geometric imperfections.

As the number of basic buckling shapes also increases with the increasing of the number of section node segments, there are a great number of basic buckling modes that can be used as initial imperfection shapes. Eight representative basic buckling shapes were selected for the following parameter analyses (shown in Fig. 7). In addition, for local buckling and distortional buckling imperfections, even with the same section buckling shapes, the imperfection fields generated in the whole columns are different if the number of half-wavelengths are different. In this section, three different buckling half-wavelength numbers were selected for local and distortional imperfection, respectively. For distortional imperfection, the number of buckling half-wavelengths can be 1, 2 and 3. For local imperfection, three cases are taken as buckling half-wavelength numbers. The number of half-wavelengths is controlled at $n \pm 5$, which is $<n$, $=n$ and $>n$, respectively. (n : the number of critical local buckling half-wavelengths of columns obtained by cFSM analysis).

Comparing the results of parameter analysis and the failure loads of

Table 8
Four different amplitudes adopted in parameter analysis.

No.	L imperfection	D imperfection	G imperfection
1	0.14t	0.64t	L/1000
2	0.34t	0.94t	L/1000
3	0.64t	1.55t	L/1000
4	1.35t	3.44t	L/1000

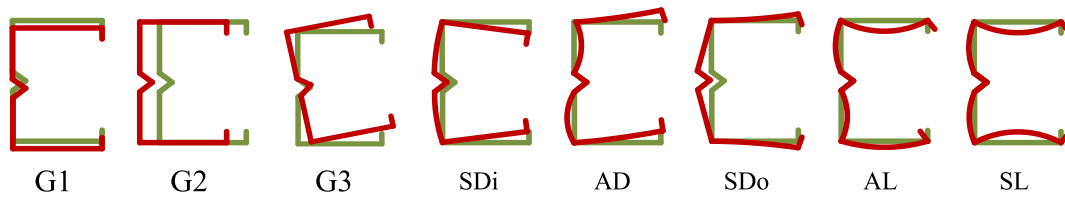


Fig. 7. Basic buckling shapes selected for parameter analysis.

members under normal conditions (P_{num}), if the ratio is greater than 1, it indicates that imperfection is helpful to improve the load-carrying capacity of members, if less than 1, indicates that imperfection will weaken the load-carrying capacity. The deviation between the ratio and 1 illustrates the influence of imperfections on the members. This study mainly showed the distributions of the minimum load-carrying capacity (P_{min}) of the members affected by various shapes imperfection within the same imperfection type and the mean value of the ratio (P_{min}/P_{FEM}). These results will help illustrate the possibility of each imperfection generating the minimum load-carrying capacity and their influence on the load-carrying capacity. The results of parameter analysis are summarized in Figs. 8–10.

5.1. Secondary local bifurcation L-D interaction

5.1.1. G geometric imperfection

Using bow, camber and twist buckling shape (denoted as G1, G2, and G3, respectively) as initial imperfection, the load-carrying capacity of fixed-ended WSLC columns under three types of global buckling imperfections was investigated. Since the number of the P_{min} caused by G3 imperfection was largest, indicating that G3 imperfection is the most likely to produce the minimum load-carrying capacity, which means that the buckling interactions in this study may be affected by the global buckling to some extent, although it has been set up $P_{cr,G}/P_{cr} > 5.2$. Moreover, compared with the other two imperfection shapes, only G3 would cause load-carrying capacity erosion.

5.1.2. D geometric imperfection

All know as, that the influence of different number of half-wavelengths on the load-carrying capacity is different although the D buckling shapes are the same, and this study came to similar conclusion. Comparing with the number of half-wavelengths along the length of the member being 1 and 3 (recorded as D-1 and D-3, respectively), the number of half-wavelengths being 2 (recorded as D-2) is more likely to lower the load-carrying capacity. Although D-2 is more likely to cause damage to the load-carrying capacity, it does not mean that D-2 imperfection will produce the greatest damage to the load-carrying capacity when compared with D-1 and D-3. On the contrary, the reduction in load-carrying capacity caused by D-1 and D-3 is larger than D-2. In addition, compared with AD-N (anti-symmetric shape), SDi-N and SDo-N (symmetric shape caused by inward and outward flange-lip motions, N presents the number of half-wavelengths) are more likely to produce the minimum load-carrying capacity and more destructive to the load-carrying capacity, and the latter is consistent with Bonada's conclusions [13].

5.1.3. L geometric imperfection

Using L buckling shape as the initial imperfection, the load-carrying capacity of the column under three types of L buckling half-wavelengths was studied. (L-2: the critical local buckling half-wavelength, L-1: the half-wavelength that smaller than L-2, and L-3: the half-wavelength that greater than L-2). Compared with L-1 and L-3, L-2 is much less likely to produce the minimum load-carrying capacity, and the load-carrying capacity deterioration caused by L-2 is not the largest. In the practical

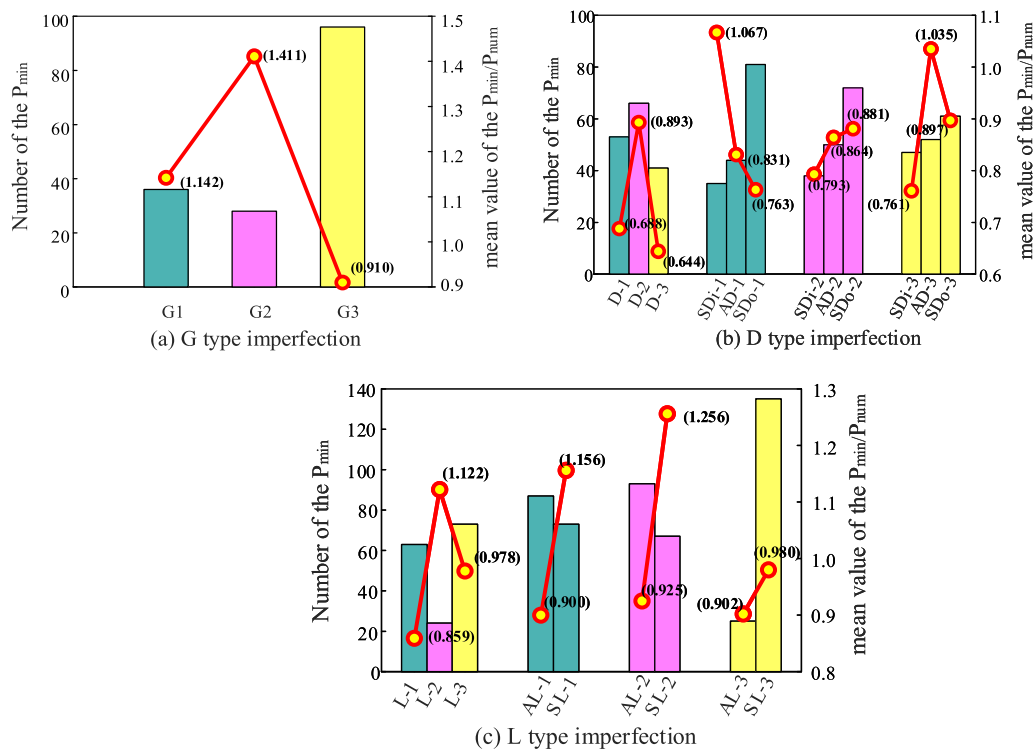


Fig. 8. Imperfection sensitivity analysis results of SLI failure.

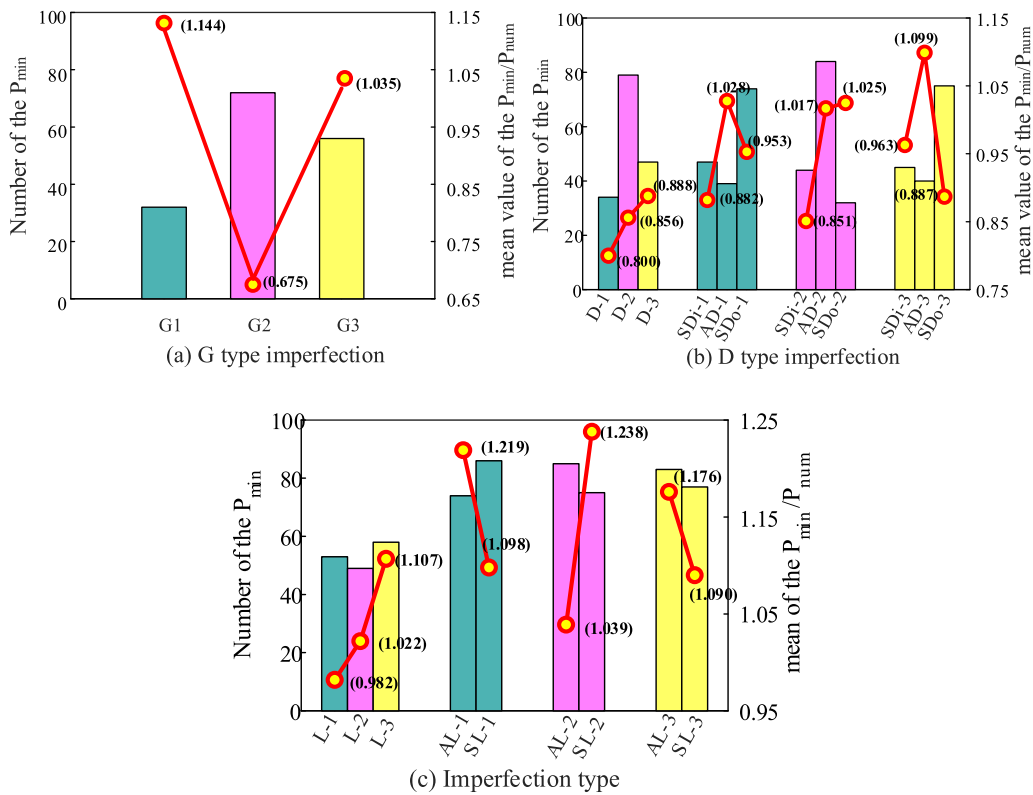


Fig. 9. Imperfection sensitivity analysis results of TI failure.

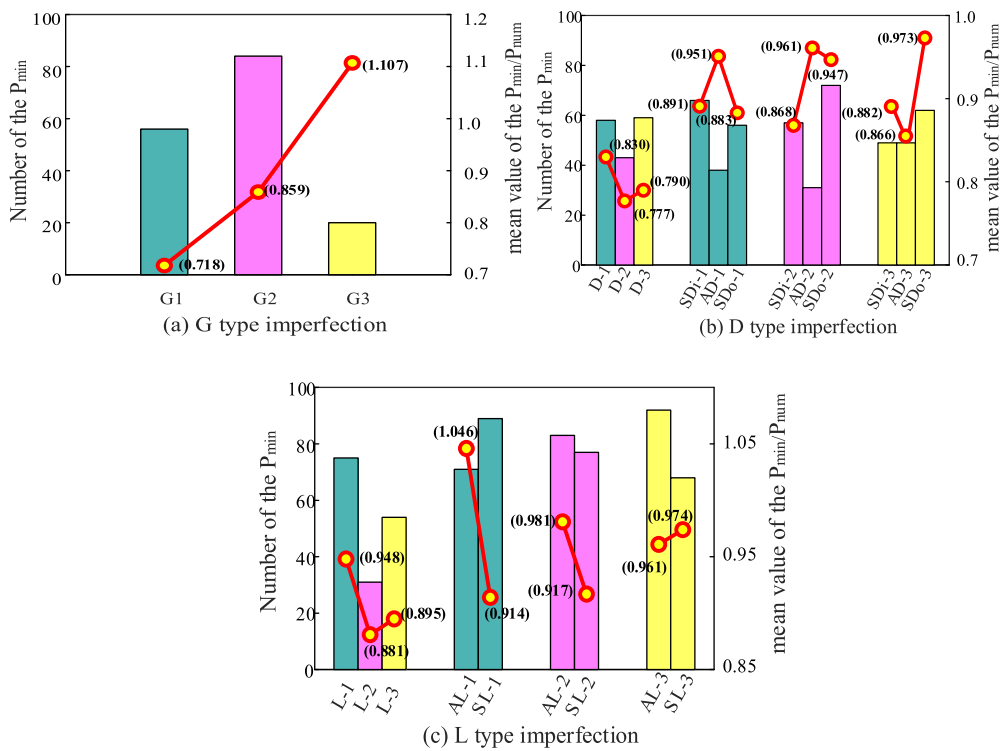


Fig. 10. Imperfection sensitivity analysis results of SDI failure.

simulation, L-2 is usually introduced as the initial L type imperfection, which may lead to failure load overestimation. Moreover, the possibility of the two shapes producing the minimum load-carrying capacity is irregular, but load-carrying capacity deterioration caused by AL-N (anti-symmetric shape, N presents the half-wavelengths of the imperfection) is

always larger than SL-N (symmetric shape).

Overall, compared with the other two types of imperfection, D geometric imperfection caused the greatest reduction in the load-carrying capacity of the fixed-ended cold-formed steel column affected by SLI failure. Especially for D-1 and D-3, the reduction of load-carrying

capacity even exceeds 30%. For D geometric imperfection, the symmetric shape imperfection has a greater negative influence on the load-carrying capacity than the anti-symmetric shape imperfection at the same half-wavelength, but the L geometric imperfection is opposite. Similar imperfection types were adopted to study the imperfection sensitivity of the load-carrying capacity of fixed-ended axial compression columns affected by TI failure and SDI failure.

5.2. True L-D interaction

5.2.1. G geometric imperfection

Fig. 9 (b) shows that G2 type imperfection is not only the easiest to produce the minimum load-carrying capacity, but also produce the largest reduction in the load-carrying capacity when compared with G1 and G3 type imperfection, which is quite different from SLI. It means that in all G geometric imperfections, G2 type imperfection is the most unfavorable for the failure load whether in terms of the probability or the degree of strength reduction.

5.2.2. D geometric imperfection

When the D buckling shape was introduced as the initial imperfection of the columns, it can be found that D-2 is most likely to generate the minimum load-carrying capacity. In addition, the strength erosion of columns caused by D-1 is the greatest. Moreover, compared with AD-N, SDi-N and SDo-N are more likely to produce the minimum load-carrying capacity when the D buckling half-wavelength is 1 and 3. The result is the opposite in the case that the D buckling half-wavelength number is 2. However, no matter what the half-wavelength of D buckling is, the failure load reduction caused by SDi-N or SDo-N is always larger than AD-N.

5.2.3. L geometric imperfection

Fig. 9 (c) illustrated that L type imperfection has little impact on the load-carrying capacity of WSLC columns experiencing TI failure. Nearly all the mean values of the numerical-to-parametric load-carrying capacity were greater than 1, which means that the L type imperfection will improve the load-carrying capacity of WSLC columns affected by TI failure. It implies that not all the initial imperfections will reduce the ultimate strength of cold-formed thin-walled steel members, which also agrees with the conclusion of Crisan [34].

In short, for the columns subjected to TI buckling failure, the initial imperfection shapes of G2 and D type have larger negative effects on the load-carrying capacity of columns, and the reduction in load-carrying capacity could reach to 32.5% and 20.0%, respectively. Moreover, for D geometric imperfection, with the same wavelength, the symmetric shape imperfection is more detrimental to the failure load than the anti-symmetric shape. As for applying L geometric imperfection, the load-carrying capacity will not decrease but will increase.

5.3. Secondary distortional bifurcation L-D interaction

5.3.1. G geometric imperfection

As can be seen from the results, compared with G3, G1 and G2 are more inclined to produce the minimum load-carrying capacity and cause greater strength reduction. Therefore, it can be concluded that G1 and G2 are more destructive to the load-carrying capacity. Especially for the G1 imperfection, its reduction in the ultimate strength reached 28.2%.

5.3.2. D geometric imperfection

Compared with D-1 and D-3, D-2 is the most destructive to the load-carrying capacity although it is least likely to produce the minimum load-carrying capacity. No matter what the imperfection half-wavelength is, AD-N type imperfection (anti-symmetric shape) is not easy to produce the minimum load-carrying capacity relative to SDi-N and SDo-N. As for the strength deterioration caused by different imperfection shapes, when the number of half-wavelengths is 1 and 2, the load-

carrying capacity reduction caused by SDi-N and SDo-N are both greater than AD-N. Although the conclusion is quite the opposite when the number of half-wavelengths is 3, it still can be found that the load-carrying capacity reduction caused by AD-3 and SDi-3 is of little difference. Therefore, it can be concluded that symmetric D buckling shape imperfection cause the biggest ultimate strength erosion of columns.

5.3.3. L geometric imperfection

As for the load-carrying capacity calculation with different L imperfections, it can be seen from the results that although there is little possibility of the minimum failure load generated by L-2 imperfection, while the reduction in load-carrying capacity caused by L-2 was the largest compared with the other two L imperfections. As for the influence of different L buckling shapes on the load-carrying capacity under the same L buckling half-wavelength, it can be found that the strength deterioration caused by the AL-N is smaller than SL-N. In the case of L-3, the reduction caused by SL-N is similar to that generated by AL-N (1.3% of difference). It can be considered that the symmetric imperfection was more detrimental for the column than anti-symmetric imperfection.

With respect to the fixed-ended axial compression columns affected by the SDI failure, the G and D geometric imperfection have larger load-carrying capacity erosion than the L buckling type, and the reduction degree is between 15% and 20%. Moreover, with the same half-wavelength, the symmetric D geometric imperfection is more destructive to the load-carrying capacity than the anti-symmetric D geometric imperfection, which is similar to the corresponding conclusion of SDI and TI failure. For the imperfection of L buckling shape, the conclusion is the opposite.

It should be pointed out that the distortional imperfection with odd half-wave (D-1 imperfection for SLI and TI failure) are the most detrimental. Although the biggest strength erosion was caused by D-2 (distortional imperfection with even half-wave) imperfection in SDI failure, it was almost identical to that caused by D-3 (distortional imperfection with odd half-wave), and the average of P_{min}/P_{num} caused by D-2 and D-3 equal to 0.777 and 0.790, respectively. What caused this different conclusion is mainly a few too low failure loads of members with D-2 imperfection, which caused a high variability and amplify the detrimental effect of the D-2 imperfection. If they were extracted from the group, the result would be similar with that of in SLI and TI failure and performed well in standard deviation (with the average/standard deviation of P_{min}/P_{num} caused by D-2 imperfection changing from 0.777/0.112 to 0.833/0.052). Furthermore, strength erosions caused by symmetric distortional imperfection (SDi and SDo) with odd half-wavelength were always the severest except for AD-3 in SDI failure due to the similar reason previously mentioned that D-2 imperfection caused the biggest strength erosion in SDI failure. These results are similar with the conclusions drew by Martins et al. [4].

6. DSM-based design approaches verification and comparison

6.1. Available DSM-based design approaches for L-D interaction

The DSM proposed by Schafer is the most widely used design approach for the cold-formed lipped channel steel members. Since it did not consider the buckling interaction, an inaccurate result is usually obtained when applied to the cold-formed steel members experiencing L-D interactive failure. Recently, several DSM-based design approaches were developed to handle with the complex section geometry shapes and buckling interaction behavior, especially for the cold-formed steel columns experiencing the L-D interaction. The approaches proposed by Schafer et al. [15] and Martins et al. [4] are widely accepted. Schafer suggested two distinct approaches for cold-formed members affected by L-D interactive failure, namely, the NLD and NDl approaches. The two approaches are given by:

$$P_{NLD} = \begin{cases} P_{ND} & \lambda_{LD} \leq 0.776 \\ \left[1 - 0.15 \times \left(\frac{P_{crL}}{P_{ND}} \right)^{0.4} \right] \left(\frac{P_{crL}}{P_{ND}} \right)^{0.4} P_{ND} & \lambda_{LD} > 0.776 \end{cases} \quad (2)$$

$$P_{NDL} = \begin{cases} P_{NL} & \lambda_{DL} \leq 0.561 \\ \left[1 - 0.25 \times \left(\frac{P_{crD}}{P_{NL}} \right)^{0.6} \right] \left(\frac{P_{crD}}{P_{NL}} \right)^{0.6} P_{NL} & \lambda_{DL} > 0.561 \end{cases} \quad (3)$$

where $\lambda_{LD} = \sqrt{P_{ND}/P_{crL}}$, $\lambda_{DL} = \sqrt{P_{NL}/P_{crD}}$, P_{crL} and P_{crD} represent critical local buckling load and critical distortional buckling load respectively, P_{NL} and P_{ND} represent local buckling capacity and distortional buckling capacity respectively.

Through the comparison with experimental data, several researchers found that NLD and NDL predictions of load-carrying capacity for fixed-ended WSLC columns affected by L-D interaction are both accurate [23], while Martins et al. [19] concluded that the NDL method is conservative. In addition, He et al. [22] applied the NLD and NDL method to predict failure loads of the cold-formed thin-walled columns described in previous literatures and found out that the accuracy and discretization of the NLD and NDL method predictions are in the same level. Moreover, Camotim et al. developed the existing DSM approach to cover the three L-D interactions. For TI and SDI failure, a generalized modified NDL approach (MNDL) and a novel approach termed NSDB were proposed, respectively. The MNDL and NSDB method can be expressed as:

$$P_{MNDL} = \begin{cases} P_{NL}^* & \lambda_{DL}^* \leq 0.561 \\ P_{NL}^* \lambda_{DL}^{*-1.2} (1 - 0.25 \lambda_{DL}^{*-1.2}) & \lambda_{DL}^* > 0.561 \end{cases} \quad (4a)$$

$$P_{NL}^* = \begin{cases} P_y & \frac{L_{crD}}{L_{crL}} \leq 8 \\ P_y + \left(2 - 0.25 \frac{L_{crD}}{L_{crL}} \right) (P_y - P_{NL}) & 8 < \frac{L_{crD}}{L_{crL}} < 12 \\ P_{NL} & \frac{L_{crD}}{L_{crL}} \geq 12 \end{cases} \quad (4b)$$

$$P_{NSDB} = \begin{cases} P_{NL} & \lambda_L \leq 0.85 \frac{P_{crD}}{P_{crL}} \\ P_1 + \frac{P_2 - P_1}{0.25} \left(\lambda_L - 0.85 \frac{P_{crD}}{P_{crL}} \right) & 0.85 \frac{P_{crD}}{P_{crL}} < \lambda_L < 0.85 \frac{P_{crD}}{P_{crL}} + 0.25 \\ P_y \lambda_L^{-1.2} (1 - 0.15 \lambda_L^{-1.2}) & 0.85 \frac{P_{crD}}{P_{crL}} + 0.25 \leq \lambda_L \end{cases} \quad (5)$$

$$P_1 = P_{y1} \times \lambda_{L1}^{-0.8} (1 - 0.15 \times \lambda_{L1}^{-0.8}) \quad (5.a)$$

$$P_2 = P_{y2} \times \lambda_{L2}^{-1.2} (1 - 0.15 \times \lambda_{L2}^{-1.2}) \quad (5.b)$$

$$\lambda_{L1} = 0.85 \times P_{crD}/P_{crL} \quad (5.c)$$

$$\lambda_{L2} = \lambda_{L1} + 0.25L \quad (5.d)$$

$$P_{y1} = \lambda_{L1}^2 \times P_{crL} \quad (5.e)$$

$$P_{y2} = \lambda_{L2}^2 \times P_{crL} \quad (5.f)$$

where L_{crL} and L_{crD} represent the half-wavelength of local buckling and distortional buckling, respectively. Through the comparison with experimental and numerical data, Dias Martins et al. [4] found that the NDL method and the MNDL method show different calculation accuracy for TI failure. Moreover, when predicting the load-carrying capacity of axial compression cold-formed steel members experiencing SDI failure, it is found that the NSDB approach outperforms the NDL approach in predicting both the experimental and numerical results.

6.2. Assessment of numerical failure load estimates

In this article, the different design approaches were used to obtain the failure load predictions of WSLC columns, and then the results were validated by the finite element results. Comparing 224 numerical analysis results of WSLC columns experiencing L-D interaction with the predictions from the NLD, NDL, MNDL, and NSDB method, the accuracy and reliability of these approaches were obtained. The modified critical half-wavelengths against the determined (numerically)-to-predicted failure load ($P_{num}/P_{prediction}$) are shown in Figs. 11–13. The load-carrying capacity deviation between the numerical results and the predictions of design approaches was measured by the dispersion between the ratio and the line: $P_{num}/P_{prediction} = 1$. The closer to the baseline the ratios were, the closer to the numerical results predictions of design approaches were, which indicated that the corresponding design approach was more accurate.

Observing Figs. 11–13, following conclusions can be drawn:

- (1) The $P_{num}/P_{prediction}$ averages/standard deviations of NLD and NDL are 0.95/0.17 and 1.04/0.19, respectively. The accuracy of the NLD and NDL method are nearly comparable and the later are more conservative for the WSLC columns experiencing SLI failure.
- (2) Similarly, the failure load predictions obtained from the NLD and NDL method for WSLC columns affected by TI failure presented the same quality of their counterparts in SLI failure, with the averages/standard deviations of P_{num}/P_{nld} and P_{num}/P_{ndl} equal to 1.02/0.24 and 0.98/0.18. The NDL method performs better in standard deviations when compared with the NLD method, although the latter is more conservative. Moreover, the MNDL method is less conservative than the other two design methods since the mean value of the P_{num}/P_{mndl} was equal to 0.84.
- (3) The three design approaches for WSLC members undergoing SDI are a little unsafe, since their averages of $P_{num}/P_{prediction}$ are all less than 1.0. The quality of the NLD and NDL method predictions is at the same level. The performance of the NSDB method in discreteness is better than the NLD and NDL method, and the standard deviation of $P_{num}/P_{prediction}$ is 0.22 in NSDB method and 0.27 in the latter two methods.

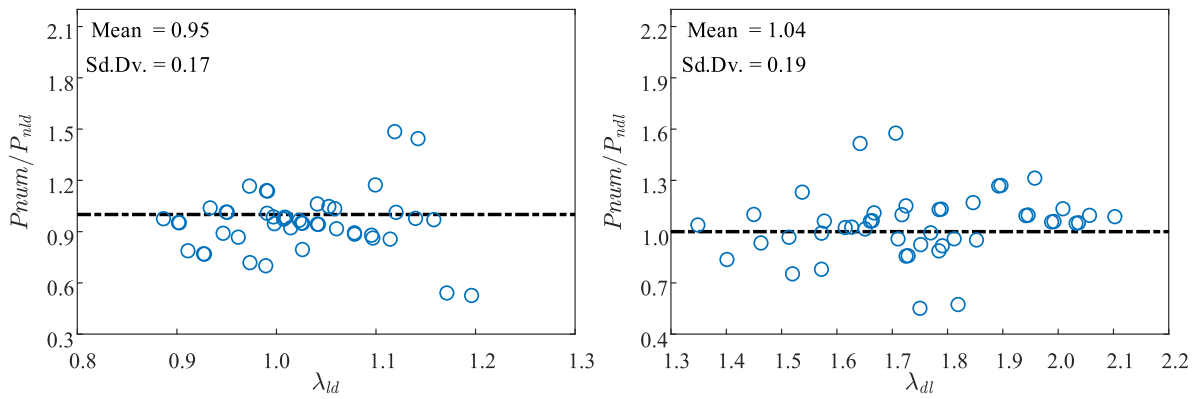
6.3. Reliability assessment

A reliability analysis was performed to assess the design method for the cold-formed WSLC steel members through the Load and Resistance Factor Design (LRFD) resistance coefficient ϕ using the expressions in Eq. (6). According to the North American Specification (NAS), the LRFD resistance coefficient ϕ recommended for compressive Cold-Formed Steel Structures members is 0.85

$$\phi = C_\phi (M_m F_m P_m) e^{-\beta_0 \sqrt{V_M^2 + V_F^2 + C_\phi V_p^2 + V_Q^2}} \quad (6)$$

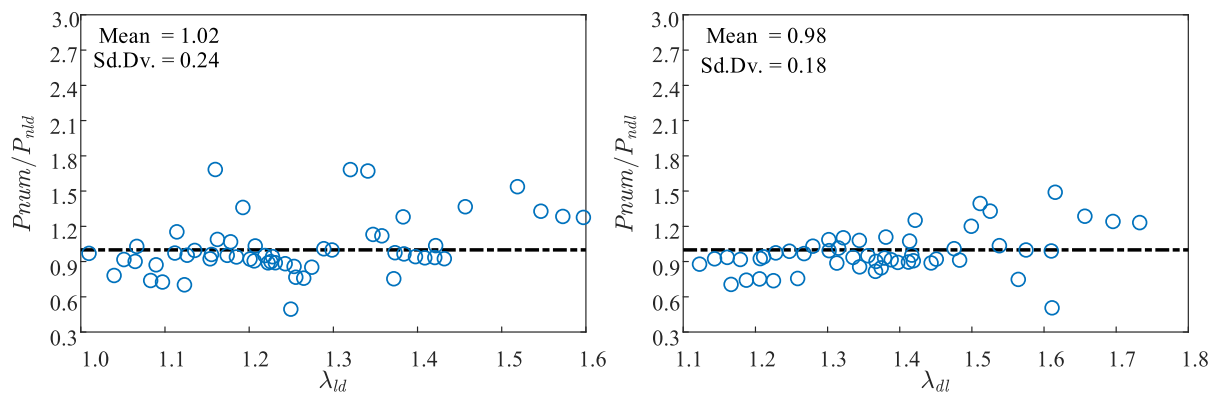
where C_ϕ : calibration coefficient for LRFD, F_m : fabrication factor mean value, β_0 : target reliability value, V_F : coefficient variation of fabrication factor, V_Q : coefficient variation of load effect, C_ϕ : a correction factor which dependent on the number of data, P_m : mean value of the 'exact'-to-predicted failure load ratios, V_p : standard deviation of the 'exact'-to-predicted failure load ratios (that's the ratio of numerical results to the predicted value), M_m : mean of the material factor, V_M : coefficient of variation of the material factor. The specific values of the coefficients are shown in Table 9, according to North American Specification AISI-S100 [30]. Table 10 presented the n , C_p , P_m , V_p and ϕ values concerning the NLD, NDL, MNDL, and NSDB failure load predictions.

The observation of the resistance coefficient in Table 10 prompts the following remarks:

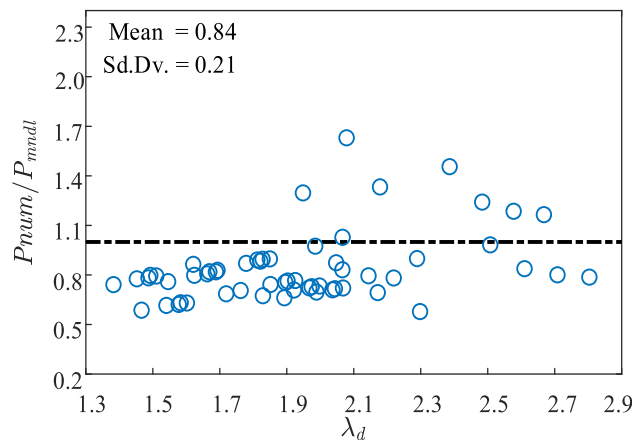


(a) Predictions of the NLD method for SLI failure (b) Predictions of the NDL method for SLI failure

Fig. 11. Predictions of DSM-based design approaches for SLI failure.



(a) Predictions of the NLD method for TI failure (b) Predictions of the NDL method for TI failure



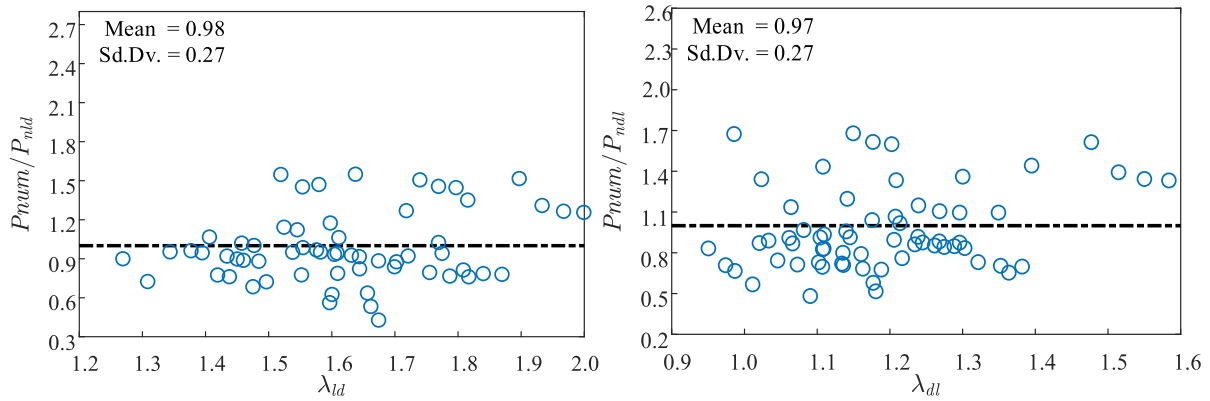
(c) Predictions of the MNDL method for TI failure

Fig. 12. Predictions of DSM-based design approaches for TI failure.

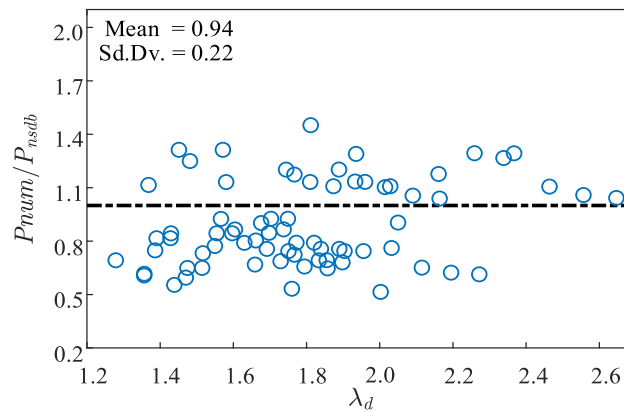
- (1) The resistance coefficient φ of the NLD, NDL method for SLI failure are equal to 1.08 and 1.14, which are both greater than 0.85. Therefore, both the two methods are conservative and the reliability of the NDL method seems to be more redundant.
- (2) As shown in Table 10, the resistance coefficients φ in the NLD, NDL and MNDL method for TI failure are all greater than 0.85 and largely different, which increase from 0.89 to 1.10. The φ in the MNDL method equals to 0.89, which is supposed to exhibit an

ideal reliability. The NLD and NDL method are too safe for designing the WSLC members undergoing TI, since they lead to $\varphi = 1.02$ and 1.10, respectively.

- (3) All the results in the NLD, NDL and NSDB method for WSLC columns affected by SDI failure are larger than 0.85, ranging from 0.92 to 0.98. The reliabilities of the numerical failure load predictions in the three design methods are all excellent.



(a) Predictions of the NLD method for SDI failure (b) Predictions of the NDL method for SDI failure



(c) Predictions of the NSDB method for SDI failure

Fig. 13. Predictions of DSM-based design approaches for SDI failure.

Table 9

The specific values of the coefficients in the resistance coefficient φ

C_φ	F_m	β_0	V_F	V_Q	M_m	V_M
1.52	1.0	2.5	0.05	0.21	1.192	0.031

7. Conclusions

In this work, the load-carrying capacity and imperfection sensitivity of cold-formed steel web-stiffened lipped channel columns subjected to the local-distortional interactive failure were studied. Combined with the theory of mode decomposition and superposition, a new imperfection simulation method was proposed. The accuracy of the proposed imperfection simulation method was verified by comparing the simulated and experimental data. Moreover, through parametric analysis, the most unfavorable imperfection for the L-D buckling failure and their

reduction in the ultimate strength were summarized. In addition, DSM-based design approaches for L-D interactive (including SLI, TI, and SDI) failure were evaluated. The main conclusions are as follows:

1. The proposed imperfection simulation method is an objective method to consider the geometric imperfections, which combines with the mode identification and decomposition theory. It is convenient and has higher accuracy than the first buckling mode method.
2. The imperfection sensitivity of the load-carrying capacity of cold-formed steel columns experiencing L-D failure was studied through parametric analysis. It was found out that:
 - (a) For the members subjected to SLI failure, the imperfection of the D buckling shape type has the greatest destructive impact on the load-carrying capacity of members and the load-carrying capacity erosion could reach 35.6%.
 - (b) For the members affected by TI failure, the imperfection of G and D buckling shape type are the most detrimental for the failure

Table 10

The resistance coefficient φ using different design approaches.

Parameter	FEM/DSM modifications								
	SLI		TI			SDI			NSDB
	NLD	NDL	NLD	NDL	MNDL	NLD	NDL		
n	46	46	55	52	58	61	65	72	
C_p	1.069	1.069	1.057	1.061	1.054	1.051	1.048	1.043	
P_m	0.95	1.04	1.02	0.98	0.84	0.98	0.97	0.94	
V_p	0.17	0.19	0.24	0.18	0.21	0.27	0.27	0.22	
φ	1.08	1.14	1.02	1.10	0.89	0.93	0.92	0.98	

loads of the members. The load-carrying capacity could even be reduced by up to 32.5%. In contrast, L geometric imperfection may be helpful to improve the ultimate strength of the members.

- (c) For members experiencing SDI failure, when compared with L geometric imperfection, G and D geometric imperfections have a greater deterioration to the failure load of the members.

Moreover, for the members subjected to L-D interactive failure, D geometric imperfection is undoubtedly the most detrimental. The strength erosion caused by the symmetric D geometric imperfection is greater than that of the anti-symmetric D geometric imperfection. For L geometric imperfection, symmetric shape imperfection is more detrimental to the members than anti-symmetric shape imperfection for SDI failure, while it is quite opposite for SLI failure. These conclusions are worth noting in practical application.

3. Through the comparison between the numerical analysis results and the predictions obtained from different design methods (NLD, NDL, MNDL, NSDB), it can be found that both the NLD and NDL method are reasonable to design the cold-formed steel columns that experience SLI. The NDL method are more appropriate for TI failure when compared with the NLD and MNDL method, and the NSDB is proposed to design WSLC columns experiencing SDI failures although it may be a bit non-conservative.

In addition, the parameter analysis in this paper only focuses on the impact of single buckling geometric imperfection on the load-carrying capacity of members, and the impact of multiple coupled buckling imperfection is not involved, which needs to be further investigated.

Declaration of competing interests

The authors declare that they have no known competing financial interests or personal relationships that could have appeared to influence the work reported in this paper.

CRediT authorship contribution statement

Lu Deng: Conceptualization, Methodology. **Jiaoli Li:** Software, Data curation, Writing - original draft. **Yuanliang Yang:** Software, Validation. **Peng Deng:** Supervision, Writing - review & editing.

Acknowledgments

The authors gratefully acknowledge the financial support provided by the Science and Technology Innovation Plan Project of Hunan Province (Grant 2018NK2053) and Changsha Excellent Innovative Youth Training Program (Project No. kq1802001).

References

- [1] B.W. Schafer, Cold-formed steel structures around the world, *Steel Constr.* 4 (2011) 141–149. <https://doi.org/10.1002/stco.201110019>.
- [2] Min Sun, Jeffrey A. Packer, Hot-dip galvanizing of cold-formed steel hollow sections: a state-of-the-art review, *Front. Struct. Civ. Eng.* 13 (2019) 49–65, <https://doi.org/10.1007/s11709-017-0448-0>.
- [3] A.D. Martins, P.B. Dinis, D. Camotim, On the influence of local-distortional interaction in the behaviour and design of cold-formed steel web-stiffened lipped channel columns, *Thin-Walled Struct.* 101 (2016) 181–204. <https://doi.org/10.1016/j.tws.2015.11.021>.
- [4] A. Dias Martins, D. Camotim, P. Borges Dinis, On the direct strength design of cold-formed steel columns failing in local-distortional interactive modes, *Thin-Walled Struct.* 120 (2017) 432–445. <https://doi.org/10.1016/j.tws.2017.06.027>.
- [5] E. Ellobody, B. Young, Behavior of cold-formed steel plain angle columns, *J. Struct. Eng.* 131 (2005) 457–466. [https://doi.org/10.1061/\(ASCE\)0733-9445\(2005\)131:3\(457\)](https://doi.org/10.1061/(ASCE)0733-9445(2005)131:3(457)).
- [6] M. Anbarasu, Mahmud Ashraf, Structural behavior of intermediate length cold-formed steel rack columns with C-stitches, *Front. Struct. Civ. Eng.* 13 (2019) 937–949, <https://doi.org/10.1007/s11709-019-0528-4>.
- [7] T. Kubiak, M. Urbaniak, G. Zucco, A. Madeo, Imperfection sensitivity analysis of the nonlinear stability of composite beams - numerical and experimental investigations, *Compos. B Eng.* 94 (2016) 360–369. <https://doi.org/10.1016/j.compob.2016.03.067>.
- [8] H.S.S. Ahmed, S. Ghosh, M. Mangal, Probabilistic estimation of the buckling strength of a CFS lipped-channel section with Type 1 imperfection, *Thin-Walled Struct.* 119 (2017) 447–456. <https://doi.org/10.1016/j.tws.2017.07.001>.
- [9] S.M. Chou, G.B. Chai, L. Ling, Finite element technique for design of stub columns, *Thin-Walled Struct.* 37 (2000) 97–112. [https://doi.org/10.1016/S0263-8d231\(00\)00018-5](https://doi.org/10.1016/S0263-8d231(00)00018-5).
- [10] B.W. Schafer, T. Peköz, Computational modeling of cold-formed steel: characterizing geometric imperfections and residual stresses, *J. Constr. Steel Res.* 47 (1998) 193–210. [https://doi.org/10.1016/S0143-974X\(98\)00007-8](https://doi.org/10.1016/S0143-974X(98)00007-8).
- [11] B.W. Schafer, Z. Li, C.D. Moen, Computational modeling of cold-formed steel, *Thin-Walled Struct.* 48 (2010) 752–762. <https://doi.org/10.1016/j.tws.2010.04.008>.
- [12] P.B. Dinis, D. Camotim, Cold-formed steel columns undergoing local-distortional coupling: behaviour and direct strength prediction against interactive failure, *Comput. Struct.* 147 (2015) 181–208. <https://doi.org/10.1016/j.compstruc.2014.09.012>.
- [13] J. Bonada, M. Casafont, F. Roure, M.M. Pastor, Selection of the initial geometrical imperfection in nonlinear FE analysis of cold-formed steel rack columns, *Thin-Walled Struct.* 51 (2012) 99–111. <https://doi.org/10.1016/j.tws.2011.10.003>.
- [14] B.W. Schafer, T. Peköz, Direct strength prediction of cold-formed steel members using numerical elastic buckling solutions, in: *Int. Spec. Conf. Cold-Formed Steel Struct. Recent Res. Dev. Cold-Formed Steel Des. Constr.*, 1998.
- [15] B.W. Schafer, Local, distortional, and Euler buckling of thin-walled columns, *J. Struct. Eng.* 128 (2002) 289–299. [https://doi.org/10.1061/\(ASCE\)0733-9445\(2002\)128:3\(289\)](https://doi.org/10.1061/(ASCE)0733-9445(2002)128:3(289)).
- [16] N. Silvestre, D. Camotim, P.B. Dinis, Post-buckling behaviour and direct strength design of lipped channel columns experiencing local/distortional interaction, *J. Constr. Steel Res.* 73 (2012) 12–30. <https://doi.org/10.1016/j.jcsr.2012.01.005>.
- [17] B. Young, N. Silvestre, D. Camotim, Cold-formed steel lipped channel columns influenced by local-distortional interaction: strength and DSM design, *J. Struct. Eng.* 139 (2013) 1059–1074. [https://doi.org/10.1061/\(ASCE\)ST.1943-541X.0000694](https://doi.org/10.1061/(ASCE)ST.1943-541X.0000694).
- [18] P.B. Dinis, B. Young, D. Camotim, Local-distortional interaction in cold-formed steel rack-section columns, *Thin-Walled Struct.* 81 (2014) 185–194. <https://doi.org/10.1016/j.tws.2013.09.010>.
- [19] A.D. Martins, P.B. Dinis, D. Camotim, P. Providência, On the relevance of local-distortional interaction effects in the behaviour and design of cold-formed steel columns, *Comput. Struct.* 160 (2015) 57–89. <https://doi.org/10.1016/j.compstruc.2015.08.003>.
- [20] Y.B. Kwon, B.S. Kim, G.J. Hancock, Compression tests of high strength cold-formed steel channels with buckling interaction, *J. Constr. Steel Res.* 65 (2009) 278–289. <https://doi.org/10.1016/j.jcsr.2008.07.005>.
- [21] D.C.Y. Yap, G.J. Hancock, Experimental study of high-strength cold-formed stiffened-web C-sections in compression, *J. Struct. Eng.* 137 (2011) 162–172. [https://doi.org/10.1061/\(ASCE\)ST.1943-541X.0000271](https://doi.org/10.1061/(ASCE)ST.1943-541X.0000271).
- [22] Z. He, X. Zhou, Z. Liu, M. Chen, Post-buckling behaviour and DSM design of web-stiffened lipped channel columns with distortional and local mode interaction, *Thin-Walled Struct.* 84 (2014) 189–203. <https://doi.org/10.1016/j.tws.2014.07.001>.
- [23] P.B. Dinis, B. Young, D. Camotim, Strength, interactive failure and design of web-stiffened lipped channel columns exhibiting distortional buckling, *Thin-Walled Struct.* 81 (2014) 195–209. <https://doi.org/10.1016/j.tws.2013.09.016>.
- [24] Dassault Systemes SIMULIA Corp. Abaqus/Standard User's Manual Version 6.14, Providence, RI, 2014.
- [25] Z. Li, B.W. Schafer, Buckling analysis of cold-formed steel members with general boundary conditions using CUFEM: conventional and constrained finite strip methods, *20th Int. Spec. Conf. Cold-Formed Steel Struct. - Recent Res. Dev. Cold-Formed Steel Des. Constr.* (2010) 17–31.
- [26] Z. Li, Stochastically simulated mode interactions of thin-walled cold-formed steel members using modal identification, *Thin-Walled Struct.* 128 (2018) 171–183. <https://doi.org/10.1016/j.tws.2017.10.012>.
- [27] S. Ádány, A.L. Joó, B.W. Schafer, Buckling mode identification of thin-walled members by using cFSM base functions, *Thin-Walled Struct.* 48 (2010) 806–817. <https://doi.org/10.1016/j.tws.2010.04.014>.
- [28] S. Ádány, B.W. Schafer, A full modal decomposition of thin-walled, single-branched open cross-section members via the constrained finite strip method, *J. Constr. Steel Res.* 64 (2008) 12–29. <https://doi.org/10.1016/j.jcsr.2007.04.004>.
- [29] European committee for standardization, Eurocode 3: Design of Steel Structures - Part 1-5: General Rules - Plated Structural Elements, 2006. <https://doi.org/10.2514/2.2772>.
- [30] A.I.S.I. Aisi-S100, North American Specification for the Design of Cold-Formed Steel Structural Members, American Iron and Steel Institute, Washington, USA, 2007.
- [31] C.H. Pham, G.J. Hancock, Direct strength design of cold-formed sections for shear and combined actions, *Proc. SDSS' Rio 2010 Int. Colloq. Stab. Ductility Steel Struct* 1 (2010) 101–114. [https://doi.org/10.1061/\(ASCE\)ST.1943-541X.0000510](https://doi.org/10.1061/(ASCE)ST.1943-541X.0000510).
- [32] D. Dubina, V. Ungureanu, Effect of imperfections on numerical simulation of instability behaviour of cold-formed steel members, *Thin-Walled Struct.* 40 (2002) 239–262. [https://doi.org/10.1016/S0263-8231\(01\)00046-5](https://doi.org/10.1016/S0263-8231(01)00046-5).
- [33] X. Zhao, M. Tootkaboni, B.W. Schafer, Laser-based cross-section measurement of cold-formed steel members: model reconstruction and application, *Thin-Walled Struct.* 120 (2017) 70–80. <https://doi.org/10.1016/j.tws.2017.08.016>.
- [34] A. Crisan, V. Ungureanu, D. Dubina, Behaviour of cold-formed steel perforated sections in compression: Part 2-Numerical investigations and design considerations, *Thin-Walled Struct.* 61 (2012) 97–105. <https://doi.org/10.1016/j.tws.2012.07.013>.